Chapter 2
Decoherence of intraband transitions in InAs quantum dots

Thomas Grange, Robson Ferreira and Gérald Bastard

Abstract The origin of the dephasing of the S-P intersublevel transitions in semiconductor quantum dots is theoretically investigated. The coherence time of this transition is shown to be lifetime-limited at low temperature, while at higher temperature pure dephasing induced by the coupling to acoustic phonons dominates the coherence decay. Population relaxation is triggered by the combined effects of electron-LO-phonon strong coupling, leading to the polaron formation, and phonon anharmonicity. A good agreement is found between the modelling and temperature dependence of the four wave mixing signal measured in recent experiments.

2.1 Introduction

Because of the discrete nature of the low-lying eigenstates in self-organised quantum dots (QDs), it was believed that these zero-dimensional objects would behave like atoms (the "macro-atom" scheme). Most of the experiments and proposals for using QDs as part of Qubits involve interband transitions where the light promotes

Thomas Grange
Laboratoire Pierre Aigrain, Ecole Normale Supérieure and CNRS, 24 rue Lhomond, F-75005 Paris, France.
Present address: Walter Schottky Institut, Technische Universität München, D-85748 Garching, Germany.
e-mail: thomas.grange@wsi.tum.de

Robson Ferreira
Laboratoire Pierre Aigrain, Ecole Normale Supérieure and CNRS, 24 rue Lhomond, F-75005 Paris, France.
e-mail: robson.ferreira@lpa.ens.fr

Gérald Bastard
Laboratoire Pierre Aigrain, Ecole Normale Supérieure and CNRS, 24 rue Lhomond, F-75005 Paris, France.
e-mail: gerald.bastard@lpa.ens.fr

G. Slavcheva and P. Roussignol (eds.), *Optical Generation and Control of Quantum Coherence in Semiconductor Nanostructures*, NanoScience and Technology 146,
DOI 10.1007/978-3-642-12491-4_2,

electrons from the full valence band to the empty conduction band, either through discrete transitions or involving the 2D (wetting layer) or 3D continuum of states. For two recent reviews on QDs, see [1, 2]. These hopes were without accounting for the solid-state aspects of the QDs, namely their coupling to the environment. The electronic degrees of freedom are intimately coupled to the vibration of the atoms and also to the randomly fluctuating electric fields due to the charging and discharging of nearby traps [3](see Chapter 3.). As a result, the macro-atom scheme survives only at very low temperature (T $\approx$ 10K or so) and the coherence of the ground interband transition decays only within a few ps at room temperature.

A very powerful coherence killer in *interband* excitation of QDs is the carrier-carrier interaction. It is known that the Auger effect is extremely efficient for excited interband transitions [3, 4]. The Auger effect however disappears if one uses intersublevel transitions in QDs doped with one electron (or one hole). Actually, an intraband transition in a one electron doped QD is a real analogue of an atomic transition in monovalent atoms.

We focus here in the intraband transitions in doped QDs. Section 2.2 briefly recalls the main aspects of the bound states of dots hosting one electron. The energetics and intrinsic lifetime (due to anharmonic couplings) of QD polaron states are discussed respectively in sections 2.3 and 2.4. Finally, section 2.5 presents very recent theoretical and experimental results of pure dephasing for intraband optical transitions involving polaron states in self-organised QDs.

2.2 Electronic states of self-organized quantum dots

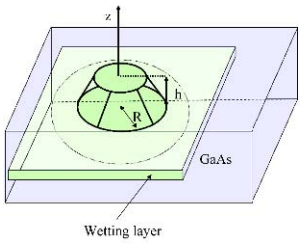

Fig. 2.1 InAs/GaAs quantum dot (schematics)

Let us therefore consider a quantum dot. The Ga(In)As/GaAs self-organised dots are known to be flat objects ($h/R \approx$ 2-3 nm/10nm where h is the dot height and R the basis radius (see Fig. 2.2 for the case of such a dot embedded in a GaAs matrix). It is also known that they are roughly circular. The electronic structure of QDs has been calculated by Stier et al [5, 6] by means of the multi-band envelope function method, while accurate atomistic approaches (pseudo-potential, tight-binding) were undertaken by Williamson and Zunger [7, 8] and by Lee et al [9].

The energy distance between the *S*-like symmetry envelope ground state in the conduction band and the centre of gravity of the P_x and P_y first excited states is typically $\approx$ 50 meV for h $\approx$ 2 nm and R $\approx$ 10 nm [10]. Figure 2.2 shows the results of a numerical computation of the envelope eigenstates of InAs QDs with cylindrical symmetry versus basis radius and maintaining the base angle constant (30°) as well as a fixed height ($h = 2.5$ nm).

One notices below the onset of the 3D GaAs continuum (taken as the energy origin) the existence of a 2D continuum. It is associated with the wetting layer on which the InAs island "floats". Being only 2.83 thick the wetting layer gives rise only to a weakly bound state for the electron z-motion: the binding energy is very small ($\approx$ 20 meV). True (*i.e.*, along the three directions) bound states, as seen in Fig. 2.2, appear for energies below E $\approx$ -20meV. The actual number of bound states in a QD is a function of its geometry (R and h) and material parameters (confining potential and effective mass). Typically, an InAs-based QD hosts three bound states for electrons in the conduction band: one ground *S*-like and two *P*-like states.

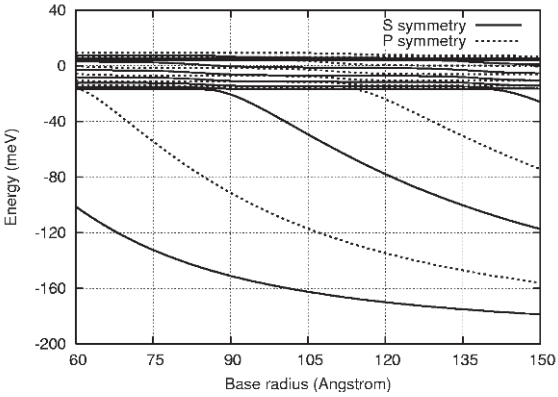

Fig. 2.2 Calculated energy levels in the conduction band of InAs/GaAs QDs versus the base radius. The dot is a truncated cone floating on a one-monolayer thick wetting layer. Solid lines: *S* levels ; dashed lines: $P\pm$ levels

In Fig. 2.2, the *P* levels are twice degenerate on account of the in-plane cylindrical symmetry. In fact, there exists a splitting between P_x and P_y ($\approx$ 5 meV) which results from potential energy terms which do not display cylindrical symmetry; for instance the ellipticity of the QD base or/and piezo-electric fields. For modulation-doped with one electron QDs, it is known [11, 12] that there exist two intraband absorptions close in energy. These two absorption lines are respectively allowed when the electric field of the light has a component along the [1,1,0] or the [1,-1,0] crystallographic axis (see Fig. 2.2.).

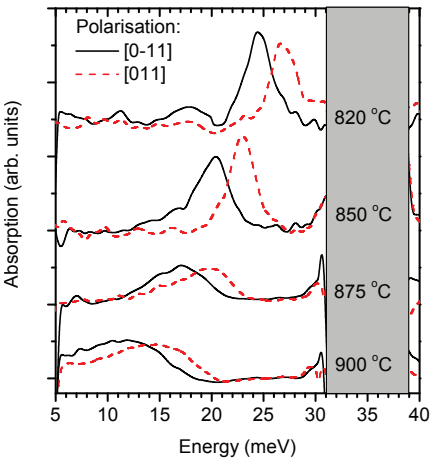

Fig. 2.3 Absorption of InAs/GaAs QDs multi stacks for different linear polarizations. The spectra correspond to QD samples that have been subjected to post-growth annealing at different temperatures. The *S*-*P* absorption lines become broader and redshifted when the annealing temperature increases.

2.3 Magneto-polaron states in charged QDs

The problem of electronic energy levels, relaxation, decoherence in QDs cannot be tackled without a deep analysis of the coupling between confined carriers and phonons. In fact, the energy relaxation problem by phonon emission (the so-called "phonon bottleneck") [13, 14, 15, 16, 17] remained unsolved until magneto-absorption experiments demonstrated that the weak coupling approach to the electron-phonon interaction in dots, leading to the phonon bottleneck effect, is a model that is essentially inapplicable to the QDs [17]. The polaronic nature of the actual elementary excitation in QDs was evidenced by magneto-optical experiments performed on stacks of InAs QDs.

The magneto-absorption technique probes the optically active eigenstates of the structures. The QDs are loaded with electrons by a controlled modulation (spike) doping of the GaAs barrier. Relaxation effects play a small role (in the magneto-absorption line broadening). The magnetic field (applied along the growth axis in the experiments) acts as a control parameter that fixes the energy distance between the ground state and the first excited electronic state. Because the zero-field size quantization is so pronounced (50 meV or so), the magnetic field acts as a perturbation to the zero-field level scheme. This is the well-known Zeeman effect in the atomic physics except that one deals with flat atoms in the case of InAs/GaAs QDs instead of spherically symmetric atoms. We deal with a orbitally non-degenerate ground state $|S\rangle$ and excited levels $|P\rangle$ which would be twice degenerate at zero-magnetic field in a circular QD (zero-field transitions in Fig. 2.3).

Under the application of a strong magnetic field parallel to the growth direction, the excited states split into $|P_+\rangle$ and $|P_-\rangle$ components (ascending and descending branches in Fig. 2.3) which are separated by the cyclotron energy $\hbar\omega_c$ ($=\hbar eB/m^*$). It is not difficult to account for a slight departure from the circularity. One finds read-

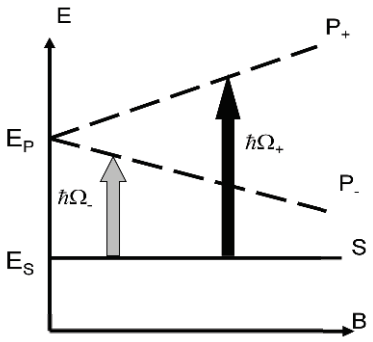

Fig. 2.4 Magnetic field dependence of the lower-lying bound states in a QD. The vertical arrows show the allowed intraband optical transitions for the two counter-rotating circular polarizations. At low temperature, only the ground *S*-like state is populated.

ily that the ground state is essentially unchanged (apart from a small diamagnetic shift) while the P_+-P_- degeneracy is lifted even at zero field :

$$\begin{aligned} \varepsilon_g(B) &= \varepsilon_S + \gamma_S B^2 \\ \varepsilon_\pm(B) &= \varepsilon_P \pm \sqrt{\left(\frac{\delta}{2}\right)^2 + \left(\frac{\hbar\omega_c}{2}\right)^2} + \gamma_P B^2 \end{aligned} \tag{2.1}$$

where δ is the zero field splitting of the P levels and γ_S and γ_P are the (small) diamagnetic contributions to the S and P states respectively. Even at B = 23T the diamagnetic terms are only a few meVs.

This description of the electronic levels and their fan dispersion under an applied magnetic field corresponds to the so-called "macro-atom" model. Within this model, illumination by far-infrared (FIR) light leads to transitions among different *electronic* levels coupled by the dipolar interaction irrespective of the other degrees of freedom, in particular the vibrations. In particular, intraband magneto-absorption experiments should display two lines at the photon energies $\hbar\omega_\pm(B) = \varepsilon_{P_\pm}(B) - \varepsilon_g(B)$ as shown in Fig. 2.3. Figure 2.3 shows the fan chart obtained on a modulation doped QD sample where the QDs contain one electron on average [18]. It is clear that the macro-atom model fails short of explaining these experimental data. In lieu of two branches $\omega_\pm$ smoothly varying with B, one finds several anti-crossings superimposed on the two branches $\omega_\pm$ of the macro-atom model. A careful analysis of the measurements demonstrates that the anti-crossings occur any time one electronic level intersects the one- or two-longitudinal optical (LO) phonon replicas of another electronic state (*i.e.*, when two macro-atom states differ by $\Delta E = n\hbar\omega_{\rm LO}$, $n = 1$ or 2 and $\hbar\omega_{\rm LO} \approx 36$ meV in GaAs and strained InAs). This experimental fact hints that a proper interpretation of the measurements should incorporate the coupling of confined electrons with optical phonons.

In order to interpret the data, a polaron model was built [18, 19] where the Fröhlich interaction $H_{\rm e-ph}$ is diagonalized between a truncated basis of factorized electron-phonon states. The latter comprises zero phonon level and LO phonon replica of the former. The LO phonons were assumed dispersionless. As a result of the diagonalization of the electron-phonon interaction, the solid lines in Fig. 2.3

were obtained. The experimental results bring evidence that over a broad energy range, typically from 15 meV to about 80 meV, $H_{\mathrm{e-ph}}$ mixes very efficiently the factorized states which differ in their electronic quantum number and in their LO phonon occupation number. In other words, it appears that in QDs the discrete nature of the electronic spectrum favors the creation of fairly stable entanglements of electronic and LO phonon states, the *polaron* states. FIR absorption experiments probe such mixed levels, instead of the purely electronic ones. This striking feature is just opposite to the findings in bulk and quantum well structures, where the electron-phonon interaction weakly couples the factorized states and, in fact, can be re-incorporated as a finite lifetime of the factorized states.

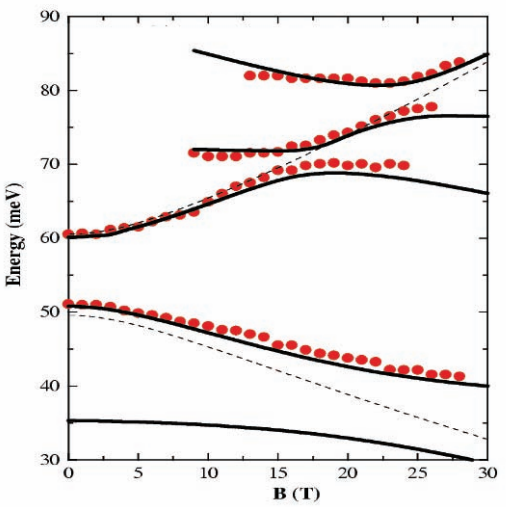

Fig. 2.5 Fan chart of magneto-optical transitions observed on stacks of InAs/GaAs QDs doped with one electron per dot on average. Dashed lines : macro-atom model. Solid lines : polaron model. Symbols : experiments (T = 4K). The reststrahlen band is around 36 meV.

2.4 Anharmonic decay of polaron states

The most important aspect of the polaron state, namely the strong coupling of states with different phonon occupancies, can be described by a simple model where only the one-phonon state $|S,1_{\mathbf{q}}\rangle$ and zero-phonon states $|P,0\rangle$ are retained in the basis. It turns out that, because LO phonons are dispersionless, the electron-phonon Hamiltonian selects one particular linear combination of $|S,1_{\mathbf{q}}\rangle$ states to hybridize with each of the discrete $|P\rangle$ state, leading to a final two-level problem. The two resulting polaron levels are then solutions of the coupled Hamiltonian:

$$\begin{pmatrix} E_P & V_{SP} \\ V_{SP} & E_S + \hbar\omega_{\mathrm{LO}} - i\Gamma_{\mathrm{LO}}/2 \end{pmatrix} \tag{2.2}$$

where V_{SP} is the Fröhlich matrix element involved, and Γ_{LO} is the broadening of the LO phonon energy due to the anharmonicity effects [20, 21, 22]. These polarons will be refered as S-P polarons in the following (P-like polaron will denote the one with a dominant P electronic component) . In fact, it is well known that bulk LO phonons have an intrinsic lifetime of a few ps. QD polarons, which are made out of bulk phonons, then become unstable entities. However, the magnitude of the anti-crossing in the magneto-optical transition $S \rightarrow P$ is much bigger than the level broadening: $2V_{SP} \approx 10meV \gg \Gamma_{\mathrm{LO}}$. Thus, the anharmonicity effects do not invalidate the polaron model, but instead contribute to its damping into two phonons according to the "chemical" equation:

$$P-\text{like polaron} \rightarrow 2 \text{ phonons} + 1 \text{ electron (S state)} \tag{2.3}$$

This polaron disintegration scheme was experimentally studied [23] recently by means of pump and probe measurements. In these experiments, a free electron laser "FELBE" in Dresden (Germany) delivers linearly polarised picosecond pulses. An initial pulse excites the single electron of a modulation doped QD from the S to the P_x or P_y state and a second pulse probes the recovery of the absorption signal for this same transition as a function of the time delay between the pump and probe pulses. The results of pump-probe experiments performed at T = 10K for different excitation energy are shown in Fig. 2.6 for annealed QDs where the polaron energies are below the Reststrahlen band (see cw spectra in Fig. 2.2). It is seen that the excited state is depleted very quickly (a few ps) near the Reststrahlen band while the relaxation time of the population in the upper state is three orders of magnitude longer when the S-P polaron energy is 14.5 meV.

The modelling of the population relaxation due to anharmonic coupling leads to a lifetime of the polaron state given by the formula [22, 23]:

$$\frac{\hbar}{\tau} = \frac{4\Delta_{SP}^2}{\left(\hbar\omega_{LO} + \Delta_{SP}\right)^2} \frac{V_{SP}^2}{\left(\hbar\omega_{LO} - \Delta_{SP}\right)^2 + V_{SP}^2} \Gamma^{ph}\left(\Delta_{SP}\right) \tag{2.4}$$

where Δ_{SP} corresponds to the optically probed transition energy between S-like and P-like polaron states with a dominant zero-phonon component. The second term in the above formula corresponds to the weight of the LO-phonon component in the excited polaron. The first term accounts for interferences between resonant and non-resonant Fröhlich interactions . The function $\Gamma^{ph}(\Delta_{SP})$ represents the broadening of the LO-phonon that one has to include in Eq. 2.2 to account for the anharmonicity effects on the polaron. It takes into account all possible disintegration paths of one LO phonon into two other phonons that occur at the polaron energy difference Δ_{SP}. For each decay channel, the relaxation rate strongly decreases with decreasing Δ_{SP}. Three factors combine to produce this decrease: the density of the two acoustic phonon states decreases steeply at low phonon energy, the amount of the one-phonon component decreases from 1/2 at resonance $\Delta_{SP} = \hbar\omega_{LO} \pm V_{SP}$ to zero

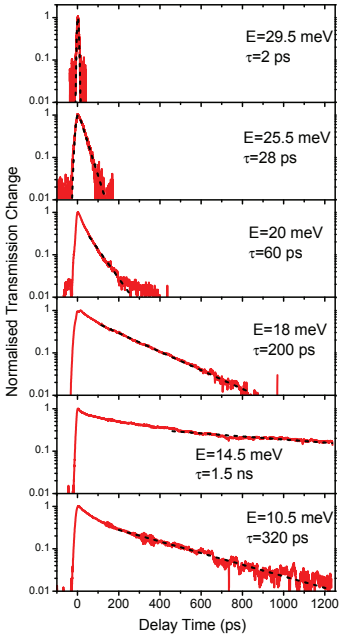

Fig. 2.6 Time dependence of the transient transmission of stack QDs in pump-probe experiments when the *S-P* energy transition is below the Reststrahlen band.

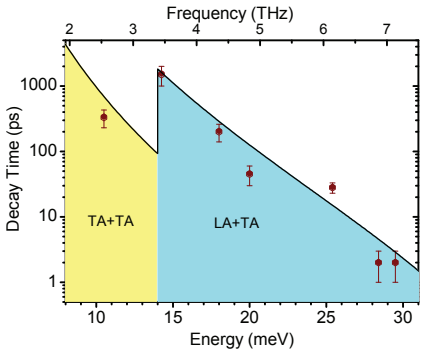

Fig. 2.7 *S-P* polaron lifetime versus polaron energy below the Reststrahlen band: experiments (symbols) and calculations (solid lines). The dominant anharmonic channels of polaron disintegration are indicated as a function of the polaron energy.

with increasing Δ_{SP} and finally the strength of the anharmonic contributions also decreases with decreasing Δ_{SP}. The important result (see Fig. 2.7.) is the very long population relaxation time of the *P*-like polaron state. This time is considerably longer than the one found in quantum well-based quantum cascade laser (QCL) devices where the relaxation involves scattering between the 2D in-plane continuum of the lasing levels. This implies that using QDs as the active medium of a QCL may prove to be more efficient in terms of population inversion than using quantum well structures.

2.5 Time resolved studies of pure dephasing in QDs

The *S-P* polaron coherent polarisation of stacked QDs has been recently studied [24] by using a two-pulse photon echo arrangement in a non-collinear geometry at the free electron laser FELIX in the Netherlands. A ratio 1:2 was used between the

two incoming pulses with wavevectors $\mathbf{k_1}$ and $\mathbf{k_2}$. The intensity of the third order non-linear signal was measured in the $2\mathbf{k_2} - \mathbf{k_1}$ direction.

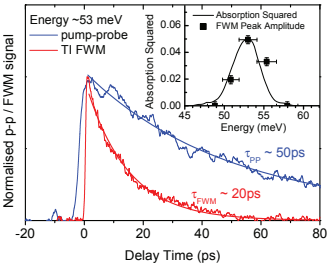

Fig. 2.8 Comparison between the four-wave mixing (FWM) and pump-probe (PP) signals for the same transition energy (53 meV) of the *S*-*P* transition. Inset: absorption squared and FWM signal intensity of the inhomogeneously broadened *S*-*P* transition.

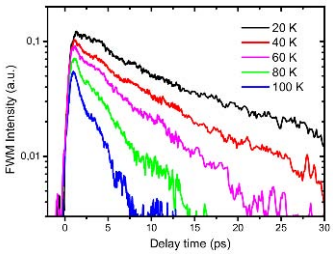

Fig. 2.9 Time dependent four-wave mixing signal (FWM) at different temperatures.

The measurements were performed in the χ^3 regime where the intensity of the four wave mixing (FWM) signal has a cubic dependence on the excitation intensity. A comparison between the FWM and the pump probe signals at the same *S*-*P* energy of 53 meV and T = 10K is shown in Fig. 2.8. Both signals decay exponentially with time constants 22 ps and 50 ps, respectively. For an inhomogeneously broadened ensemble of two-level systems, it is known that the coherence lifetime T_2 is equal to four times the decay time of the FWM signal. Hence, at low temperature, $T_2 \approx 90$ ps is nearly twice $T_1 = 50$ ps, the population relaxation time which is the ultimate limit when the pure dephasing processes are negligible. This is no longer the case when the temperature increases, as shown in Fig. 2.9. The decay time of the FWM signal decreases very steeply with increasing temperature (from 22 ps at T = 10K to 3ps at T = 100K) while the population relaxation time varies much less. This indicates that the pure dephasing processes become dominant when the temperature increases. Such feature is the same as found in the case of the interband transitions [25, 26].

In order to analyze the magnitude and temperature dependence of the coherence time, we have to use the polaron description of the QD eigenstates. However, the intrinsic anharmonicity driven decay of the QD electron and LO-phonon entanglement explains the measured decay only at low temperature. At high temperatures, this decay channel is far too ineffective to be compatible with the observations. Hence, other sources of decoherence have to be invoked to explain the data. Since there is a strong temperature dependence even below 30K, the interaction with the acoustic phonons has to be taken into account. Two contributions show up. (i) Firstly, the acoustic phonon sidebands will contribute to a partial loss of coherence. The phonon sidebands, first analyzed by Huang and Rhys [28], arise from the fact that the equilibrium positions of the atoms are not exactly the same when the electron

is in the excited or ground states, because of the electron - acoustic phonon interaction. In our case we deal with *S*-*P* or *S* polarons but the physics is identical. Since the equilibrium positions are different, there can be electronic optical transitions, triggered by the dipolar coupling to the light, that take place with different phonon occupancies. This is because the phonon wavefunctions (Hermite functions) are not centered at the same origin and, consequently, two phonon wavefunctions that correspond to different phonon occupancies are no longer orthogonal. (ii) In addition, the optically probed *S*-P_x polaron state is close (a few meVs) in energy from the (*S*-P_y) polaron state. Therefore, acoustic phonon absorption and emission processes become allowed between these two polaron states. Thus, thermally stimulated escape of a photo-excited carrier from the lower *S*-P_x to the upper *S*-P_y polaron state becomes possible and will contribute to the loss of coherence of the *S*-P_x related transition. In addition, virtual transitions to the other *P*-like polaron (P_y) state do also have to be considered. These virtual transitions can be considered as a scattering by acoustic phonons thereby inducing a virtual excursion of the polaron to another *S*-*P* polaron state through off-diagonal elements of the deformation potential coupling. Virtual transitions do not change the electron populations, but create interactions between the two electronic states involved in the optical transition and the phonon bath, and thus contribute also to the loss of coherence of the optical transition.

In the following, we consider the interaction between the polarons and the longitudinal acoustic phonons via the deformation potential approximation:

$$V = \sum_{i,j} \sum_{q} M_q^{i,j} \left(a_q + a_{-q}^{+} \right) |i\rangle\langle j| \quad ; \quad M_q^{i,j} = D_c \sqrt{\frac{\hbar q}{3\rho c_s \Omega}} \langle i | e^{iq.r} | j \rangle \tag{2.5}$$

The diagonal components correspond to the Huang-Rhys term and will give rise to the acoustic phonon sidebands while the off-diagonal terms that involve the polarons *S*-P_x and *S*-P_y will lead, at the lowest order in V, to the thermal escape of the carrier from the upper state involved in the optical transition. Higher order terms will contribute to the virtual transitions. For the interaction with the acoustic phonons, and far away from the polaron resonance, the electronic components play a more important role than the phonon component (this is exactly the reverse of the population relaxation case where only the one LO phonon part of the polaron wavefunction matters). Hence, from now on we consider only the *S*, P_x and P_y states. The diagonal components $|S\rangle\langle S|$ and $|P\rangle\langle P|$ involve the same deformation potential D_c since both states belong to the conduction band. This is in striking contrast with the sidebands observed in interband transitions where the initial and final electron states display deformation potentials that have opposite signs. Let us introduce the unperturbed acoustic phonon Hamiltonian:

$$H_{ph} = \sum_{q} \hbar \omega_q \left(a_q^{+} a_q + \frac{1}{2} \right) \tag{2.6}$$

We see that the diagonal terms of the electron-phonon interaction can separately be diagonalized when H_{ph} is added. In fact, let us define the new phonon operators:

$$b_q^+ = a_q^+ + \frac{M_{i,q}^*}{\hbar\omega_q} = a_q^+ + S_{i,\bar{q}}^* \quad ; \quad M_{i,q} = M_q^{i,i} = D_c\sqrt{\frac{\hbar q}{3\rho c_s \Omega}}\langle i|e^{iq.r}|i\rangle \quad (2.7)$$

Then, the complete Hamiltonian $H_{ph}+V$ can be exactly diagonalized like:

$$H = H_{ph}+V = \sum_q \hbar\omega_q\left(b_q^+ b_q + \frac{1}{2}\right) - \sum_q \frac{\left|M_{i,q}\right|^2}{\hbar\omega_q} \quad with \quad i = S,P \quad (2.8)$$

As expected the phonons have kept the same vibration frequencies (displacing an harmonic oscillator does not affect its eigenfrequency). But the phonon wavefunctions are not the same. The new eigenstates are:

$$\left|\tilde{n}_q\right\rangle = \frac{\left(b_q^+\right)^n}{\sqrt{n!}}\left|\tilde{0}_q\right\rangle \quad ; \quad \left|\tilde{0}_q\right\rangle = \exp\left(-\frac{S_{i,q}^2}{2}\right)\exp\left(-S_{i,q}a_q^+\right) \quad (2.9)$$

Because of the modification of the phonon states, the intraband optical spectrum related to the *S*-*P* transition can now occur with or without conservation of the phonon occupancy. The phonon conservation gives rise to the zero phonon line (ZPL) and the transitions that involve emission or absorption of one or several phonons give rise to the phonon sidebands. Let us denote by ε the detuning with respect to the purely electronic contribution $\varepsilon_P - \varepsilon_S$. Then the absorption lineshape is given by [24]:

$$A(\varepsilon) = Ze^f(\varepsilon) \quad ; \quad e^f(\varepsilon) = \delta(\varepsilon) + f + \frac{f\otimes f}{2} + ... \quad (2.10)$$

where the exponential function is taken in a convolution sense, $f(\varepsilon)$ is the function:

$$f(\varepsilon) = \sum_q \frac{\left|M_q^{P_xP_x} - M_q^{SS}\right|^2}{\varepsilon^2}\left[N(|\varepsilon|) + \Theta(\varepsilon)\right]\delta(|\varepsilon| - \hbar\omega_q) \quad (2.11)$$

and Z is the weight of the zero phonon line:

$$Z = \exp\left(-\int_{-\infty}^{+\infty} d\varepsilon f(\varepsilon)\right) \quad (2.12)$$

In Eq. 2.10, the i^{th} term corresponds to a transition that involves i-phonon processes (absorption and/or emission). It can be checked that $A(\varepsilon)$ is normalized to 1 and that it can also be rewritten as:

$$A(\varepsilon) = \frac{1}{h}\int_{-\infty}^{+\infty} dt e^{-i\frac{\varepsilon t}{\hbar}}\exp\left[\int_{-\infty}^{+\infty} d\varepsilon' f(\varepsilon')\left(e^{-i\frac{\varepsilon' t}{\hbar}} - 1\right)\right] \quad (2.13)$$

which is the Fourier transform of the time evolution of the *S*-*P* coherence [29]. A calculation of $A(\varepsilon)$ convolved with a Lorentzian of linewidth Γ_2 (see below) is shown in Fig. 2.5. The shape differs considerably from the one found for interband transitions. Note that the phonon wings have two clear maxima, which are separated by ≈ 3 meV. Hence they are likely to give rise to observable features in the time evolution of the FWM signal if the damping is not too large. The physical origin of this salient property of the coupling to the acoustic phonons in intraband transitions is the fact that the same deformation potential affects the initial and final states, while different deformation potentials control the electron-phonon couplings in the conduction and valence bands.

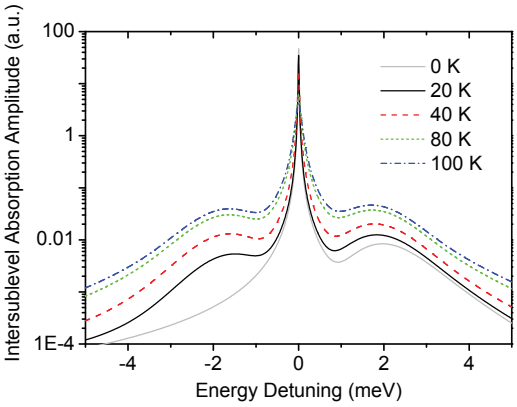

Fig. 2.10 Calculated absorption lineshape of the *S*-*P* intersublevel transition versus energy detuning with respect to the zero phonon line (ZPL).

Figure 2.5 shows the time evolution of the FWM signal at different temperatures. We see that the exponential decay is more and more pronounced when T increases. We do see a small feature near 2 ps that we attribute to the peculiar double maxima in the absorption curve versus energy.

The exponential decay of the FWM signal cannot be accounted for only by the diagonal part of the electron-phonon interaction. The ZPL is in this approximation unbroadened and therefore there is only a partial loss of coherence due to the diagonal coupling. In order to obtain further decoherence, we need to take into account thermal escape from the excited state of the transition (the thermal escape from the ground state is negligible for *S*-*P* transition energies in the 50 meV range). In fact there are two *P* levels that are as close as a few meVs. After a delta excitation pulse, the FWM signal is given by the expression:

$$I(t) \propto \Theta(t) \exp\left[-2\Gamma_2 t - 16 \int_{-\infty}^{+\infty} d\varepsilon f(\varepsilon) \sin^2\left(\frac{\varepsilon t}{2\hbar}\right)\right] \tag{2.14}$$

The broadening Γ_2 can be decomposed in $\Gamma_2 = \hbar/\tau + \Gamma_2^*$, where τ is the anharmonic polaron decay time to the ground state (Eq. 2.4), and Γ_2^* has been calculated by taking into account the off-diagonal part of the electron-phonon interaction up

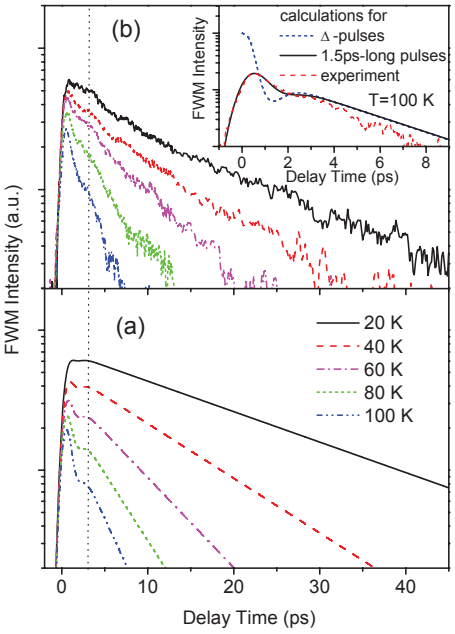

Fig. 2.11 Temperature dependent FWM signal. (a) Simulations. (b) Experiments. Inset: Calculated FWM signal at 100K for a delta pulse and for a 1.5ps duration pulse compared to the experimental data.

to two-phonon processes [24, 27]. The one-phonon processes correspond to the absorption of an acoustic phonon from the lower P level to the upper one while the two-phonon processes are virtual transitions between the two P levels. We found:

$$\Gamma_2^* = \frac{1}{2\pi}\int_0^\infty d\varepsilon \frac{4\Delta_{PP}^2}{(\varepsilon+\Delta_{PP})^2} \times \frac{\Gamma_{PP}^2(\varepsilon)N(\varepsilon)[N(\varepsilon)+1]}{(\varepsilon+\Delta_{PP})^2+\left(\frac{\Gamma_{PP}(\varepsilon)[N(\varepsilon)+1]}{2}\right)^2} \tag{2.15}$$

where

$$\Gamma_{PP}(\varepsilon) = \frac{2\pi}{\hbar}\sum_q \left|M_q^{P_xP_y}\right|^2 \delta(\varepsilon-\hbar\omega_q) \tag{2.16}$$

and $N(\varepsilon)$ is the Bose distribution function. It is the pole at Δ_{PP} that corresponds to the absorption of one acoustic phonon while phonons that are not resonant with Δ_{PP} give rise to the virtual transitions between the two P levels. One can show that the phonons with energies between 2 and 3 meV contribute the more to these virtual transitions and their contribution to the dephasing is proportional to $N(\varepsilon)[N(\varepsilon)+1]$. Therefore, the real or virtual transitions between the two P levels depend strongly on temperature. This is illustrated in Fig. 2.5 where the homogeneous linewidth is plotted versus T. One sees that the contributions of the virtual and real transitions to the dephasing are comparable up to 60K. However, above 60K the virtual transitions are prevalent. The measured and calculated linewidths are in good agreement. Γ_2

increases rapidly from 15meV at 10K to 150 meV when T = 120K. This is in marked contrast with the population relaxation time (dotted line in Fig. 2.5.

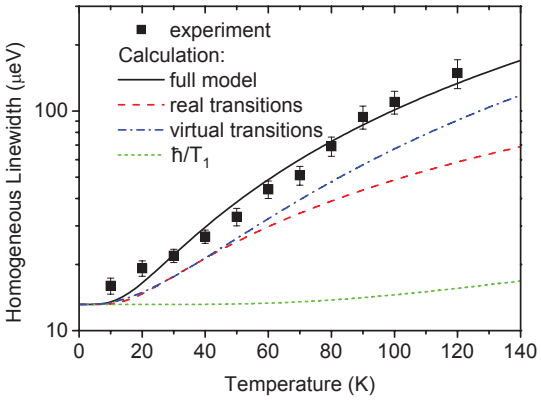

Fig. 2.12 Temperature dependence of the *S-P* transition linewidth: experiments (closed squares) and calculations including real and virtual transitions between the *P* states. The dotted line accounts for the population relaxation (time T_1) from the upper to the lower state of the transition.

2.6 Conclusion

Time resolved pump and probe and degenerate four-wave mixings experiments have been performed on ensemble of InAs/GaAs self-organized QDs. Experiments clearly show that the energy relaxation in these zero-dimensional objects is of different nature from the one found in bulk and quantum well materials. The formation of polarons between electrons and LO phonons invalidates the usual energy relaxation scheme, namely the irreversible emission of LO phonons by the excited electrons. In QDs the energy relaxation proceeds via the anharmonicity-triggered disintegration of the polarons. The polaron model has proven to be in quantitative agreement with experiments when the QD size increases and makes the S-P transition energy to become smaller than the longitudinal optical phonon energy. Very long (ns) relaxation times for electrons in the excited states are found in these broad dots. The coherence of the S-P transition energy has been measured and calculated versus temperature. The coherence of intraband transitions behaves in a similar way as found in the case of interband experiment. It is only at very low temperature, say $T < 10K$, that the pure dephasing mechanisms can be safely neglected.

Acknowledgements The LPA-ENS is UMR-8551 CNRS and is "Unité associée aux Universités Paris 6 et Paris 7". We are very pleased to acknowledge fruitful collaborations with Drs. E. Zibik, L. Wilson and M. Skolnick at Sheffield University (UK) and the FELIX and FELBE free electron laser facilities and their collaborators.

References

1. *Semiconductor Macroatoms. Basic Physics and Quantum device Applications.* Edited by F. Rossi. Imperial College Press. London (2005).
2. Ferreira R., Berthelot A., Grange T., Zibik E., Cassabois G. and Wilson L., Journ. Appl. Phys. **105**, (2009).
3. Bockelmann U. and Egeler T. Electron relaxation in quantum dots by means of Auger processes. Phys Rev. B **46**, 15574 (1992)..
4. Ferreira R. and Bastard G. Phonon-assisted capture and intradot Auger relaxation in quantum dots. Appl. Phys. Lett. **74**, 2818 (1999).
5. Stier O., Grundmann M. and Bimberg D. Phys. Rev. **B59**, 5688 (1999).
6. Stier O. *Electronic and Optical Properties of Quantum dots and Wires.* Berlin Studies in Solid State Physics. Wissenshaft & Teknik. Verlag. Berlin (2001).
7. Williamson A. J. and Zunger A. Phys. Rev. B **59**, 15819 (1999) and **61**, 1978 (2000).
8. Zunger A. Phys. Stat. Sol.A **190**, 467 (2002) and references cited therein.
9. Lee S., Jönsson L., Wilkins J. W. , Bryant G. W., Klimeck G. Phys. Rev. B **63**, 195318 (2001).
10. Frey F., Rebohle L., Muller T., Strasser G., Unterrainer K., N'guyen D. P., Ferreira F. and Bastard G. Bound-to-bound and bound-to-continuum optical transitions in combined quantum dot-superlattice systems. Phys. Rev. B **72**, 155310 (2005).
11. Sauvage S. et al. Long polaron lifetimein InAs/GaAs self assembled quantum dots. Phys. Rev. Lett. **88**,177402 (2002).
12. Zibik E. A. et al. Intraband relaxation via polaron decay in InAs self assembled quantum dots. Phys. Rev. B **70**, 161305 (R) (2004).
13. Bockelmann U. and Bastard G. Phonon scattering and energy relaxation in two- , one- and zero-dimensional electron gases. Phys. Rev. B**42**, 8947 (1990).
14. Benisty H., Sotomayor-Torres C. M. and Weisbuch C. Intrinsic mechanism for the poor luminescence of quantum box systems. Phys. Rev. B **44**, 10945 (1991).
15. Urayama J. , Norris T. B. , Singh J. and Bhattacharya P. Observation of phonon bottleneck in quantum dot electronic relaxation. Phys. Rev. Lett. **86**, 4930 (2001).
16. Murdin B. N. et al. Direct observation of the LO phonon bottleneck in wide GaAs / Ga1-xAlxAs quantum wells. Phys. Rev. B **55**, 5171 (1997).
17. Inoshita T. and Sakaki H. Density of states and phonon induced relaxation of electrons in semiconductor quantum dots. Phys. Rev. B **56**, R4355 (1997).
18. Hameau S. et al. Strong electron-phonon coupling regime in quantum dots: evidence for everlasting resonant polarons. Phys. Rev. Lett. **83**, 4152 (1999).
19. Ferreira R. and Bastard G. Electron-phonon interaction in Semiconductor Quantum Dots. in *Semiconductor Macroatoms. Basic Physics and Quantum device Applications.* Edited by F. Rossi. Imperial College Press. London (2005).
20. Li X. Q., Nakayama H. and Arakawa Y. Phonon bottleneck in quantum dots: Role of the lifetime of the confined optical phonons. Phys. Rev. B **59**, 5069 (1999).
21. Verzelen O. Ferreira R. and Bastard G. Polaron lifetime and energy relaxation in semiconductor quantum dots. Phys Rev. B **62**, 4809 (2000).
22. Grange T., Ferreira R. and Bastard G. Polaron relaxation in self assembled quantum dots: breakdown of the semiclassical model. Phys. Rev. B **76**, 241304 (2007).
23. Zibik A., Grange T., Carpenter B. A., Porter N. E., Ferreira R., Bastard G., Stehr D., Winnerl S., Helm M., Liu H. Y., Skolnick M. S. and Wilson L. R. Long lifetimes of quantum-dot intersublevel transitions in the terahertz range. Nature Materials **8**, 803 - 807 (2009).
24. Zibik E. A. et al Intersublevel polaron dephasing in self assembled quantum dots. Phys. Rev.B **77**, 041307(R) (2008).
25. Borri P., Langbein W, Schneider S., Woggon U., Sellin R. L., Ouyang D. and Bimberg D. Phys. Rev. Lett. **87**, 157401 (2001).
26. Borri P. and Langbein W. Four wave mixing dynamics of excitons in InGaAs self-assembled quantum dots. J. Phys. Condens. Matter **19**, 295201 (2007).

27. Grange T. Decoherence in quantum dots due to real and virtual transitions: A nonperturbative calculation. Phys. Rev.B **80**, 245310 (2009).
28. Huang K. and Rhys. A. Theory of light absorption and non radiative transitions in F centres. Proc. R. Soc. London ser A **204**, 406 (1950).
29. Vagov A., Axt V. M., Kuhn T., Langbein W., Borri P. and Woggon U. Nonmonotonous temperature dependence of the initial decoherence in quantum dots. Phys. Rev. B **70**, 201305 (2004).

http://www.springer.com/978-3-642-12490-7

Optical Generation and Control of Quantum Coherence in Semiconductor Nanostructures

Slavcheva, G.; Roussignol, P. (Eds.)

2010, XX, 338 p. 150 illus., 5 illus. in color., Hardcover
ISBN: 978-3-642-12490-7